Academic Journal of Science and Technology
ISSN: 2771-3032 | Vol. 13, No. 3, 2024

Dynamic Response and Stability Analysis of Anti-slide Pile Reinforced Slopes under Earthquake Conditions

Longqian Zhang

Department of civil engineering Yunnan University, Yunnan, China

Abstract: This paper examines the seismic stability of a slope located in Shimian County, Ya'an City, Sichuan Province. The earthquake activity level in the area is classified as VIII, with a designed peak acceleration of 0.3g. A three-dimensional finite element model was established using ABAQUS to analyze the effects of different amplitudes of Wenchuan earthquake waves (0.1g, 0.2g, 0.3g) on the skid pile slope. Research has found that as the intensity of seismic waves rises, the peak seismic acceleration and displacement at various monitoring locations on the slope surface also grow, and the amplification effect becomes more significant at higher altitudes. In addition, the peak horizontal displacement in the x-direction at different elevations of the slope surface also increases with the rise in seismic wave amplitude The first principal stress of the skid pile is mainly concentrated near the connection between the sliding surface and the skid pile, and the peak stress increases with the amplitude of seismic waves. Research has shown that the stability coefficient of skid piles under 0.3g earthquake conditions is lower than the standard requirements, indicating that using skid piles alone may not be sufficient to ensure slope stability. Recommendations to strengthen or resize the structural design.

Keywords: Anti-slide pile; Stability; Seismic load; Numerical simulation.

1. Introduction

Skid pile is a commonly used method to enhance slope stability, [1] especially in improving its seismic performance. However, there is relatively little studies on the design of anti-slip piles, especially in the exploration of stress changes inside the pile under earthquake conditions. [2] Since the 1995 Hanshin earthquake in Japan, foreign researchers have begun to use dynamic centrifugal simulation tests to explore the effects of liquefaction and lateral displacement caused by earthquakes on the bending moment and deformation of piles. [3] Representative scholars include Brandenberg, Abdoun, and J Boulanger et al. [4] However, it should be noted that these studies mainly focus on pile foundations, which differ significantly from skid piles used as supporting structures. At present, research on the reaction to dynamic forces of skid piles in China is still limited. After the Wenchuan earthquake on May 12th, many skid pile support structures suffered varying degrees of damage. [2] Due to the lack of research data on the interaction mechanism between skid piles and deformed slopes under earthquake action in China. Considerable uncertainty exists in the design of anti-slip piles for disaster recovery and regions prone to earthquakes. Unable to accurately evaluate the rationality and effectiveness of design measures, as well as the degree of optimization of design schemes. Therefore, this study uses ABAQUS finite element calculation software to investigate the dynamic response of skid pile reinforced slopes under earthquake action, taking an actual case of skid pile reinforcement as the object, and using artificial seismic waves. The aim is to reveal the displacement and internal force changes of various parts of the pile body during the earthquake process, and provide theoretical support for the design of skid piles under earthquake action.

2. Basic Theory

2.1. Strength Reduction

The strength reduction approach decreases the shear strength parameters c and ϕ of the slope's rock mass by a factor FS until the slope becomes unstable, with the corresponding FS being the slope stability coefficient. The slope stability coefficient is expressed as:[5]

$$\tau = \mathrm{c} + \tan\phi \tag{1}$$

After strength reduction, it can be obtained that:

$$\tau' = \mathrm{c}' + \tan\phi' \tag{2}$$

$$\mathrm{c}' = \frac{\mathrm{c}}{\mathrm{F_s}} \tag{3}$$

In summary, we have:

$$\tan\phi' = \frac{\tan\phi}{F_s} \tag{4}$$

Where: c and ϕ represent the initial parameters of the slope's rock and soil mass;c′and ϕ′represent the parameters when the slope's rock and soil mass reach the limit equilibrium state;FS represents the stability coefficient of the slope.

2.2. Modal Analysis Theory

Modal analysis examines the inherent characteristics of the structure, such as stiffness, natural frequency, and mode shape, before conducting dynamic analysis. Essentially, modal analysis involves solving the eigenvectors and eigenvalues of the structure.[6]

The equation for undamped free vibration is:

$$[\mathrm{M}]\{\ddot{\mathrm{x}}\}+[\mathrm{K}]\{x\}=\{0\} \tag{5}$$

Assuming the solution to the equation is:

$$\{x\}=\{u\}\sin(\omega t-\phi) \tag{6}$$

Substituting into the equation, we get:

$$([\mathrm{K}]-\omega^2[\mathrm{M}])\{\mathrm{u}\}=\{0\} \tag{7}$$

For the above equation to have a solution, the condition must be met $([\mathrm{K}]-\omega^2[\mathrm{M}])=\{0\}$,which constitutes the characteristic equation. Based on the characteristic equation, nnn characteristic roots (i.e., natural frequencies) can be obtained (i = 1, 2, ..., n). ω_i^2 (i=1,2,……,n),Substituting the characteristic roots into equation (7),yields the corresponding non-zero vectors $\{\mathrm{u}^{(i)}\}$(i.e., mode shapes).

3. Engineering Overview

A slope is situated in Shimian County, Ya'an City, Sichuan Province. Under the action of tectonic compression, the ridge is steep, with slope angles between 30° and 38°. The area belongs to an erosion-type canyon landscape with many V-shaped gullies and river erosion-deposition topography. The area experiences a subtropical humid monsoon climate, with most rainfall occurring during the summer and autumn seasons. The area is also prone to earthquakes, with frequent fault activities of varying scales. This region falls within a high seismic risk zone, with a fundamental seismic intensity rated at VIII degree and a design peak ground acceleration set at 0.3g.

4. Calculation Model

4.1. Establishment of Numerical Model

The ABAQUS finite element software is utilized to model the slope and anti-slide piles, as depicted in Figure 1. The overall dimensions of the slope model are 60m (length) × 10m (width) × 25m (height at slope bottom), with a top height of 50m. The soil layers from top to bottom are fractured limestone, slightly to weakly weathered limestone, and intact limestone. The relevant rock mass parameters are provided in Table 1.The anti-slide piles are 28m long and have a diameter of 2×3m, with a spacing of 3m. Monitoring points A, B, and C are set on the slope surface (see Figure 1).

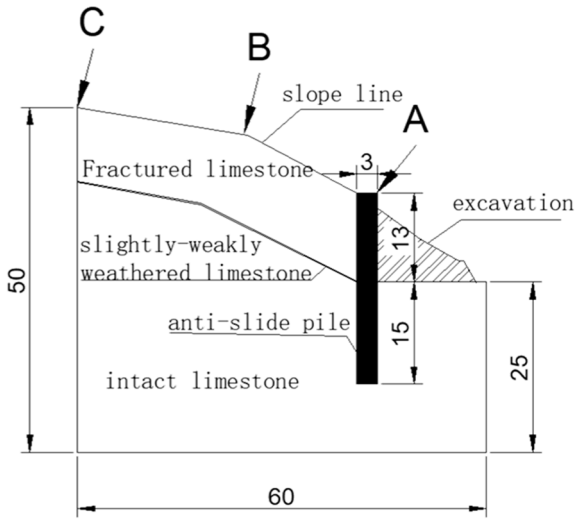

Figure 1. Layout of Anti-slide Pile Support

Table 1. Physical and Mechanical Properties of Slope Rocks and Skid Piles

Name	Density ρ/g·cm-3	Poisson's Ratio μ	Elastic Modulus E/GPa	Cohesion c/kPa	Internal Friction Angle φ/()°
Anti-slide Pile	2.5	0.25	35	—	—
Fractured Limestone	2.3	0.3	2.8	500	26
Slightly to Weakly Weathered Limestone	2.5	0.25	15	1200	32
Intact Limestone	2.65	0.22	35.4	1900	41

4.2. Parameter Selection and Boundary Conditions

Considering the elastoplastic characteristics of the soil, the Mohr-Coulomb plastic constitutive model is adopted for the slope rock mass. Rayleigh damping is used to achieve kinetic energy decay, expressed as:

$$[\mathrm{C}]=\alpha[\mathrm{M}]+\beta[\mathrm{K}] \tag{8}$$

In this context, [C] represents the damping matrix, [M] the mass matrix, and [K] the stiffness matrix, while α and β are the mass-related and stiffness-related damping coefficients, respectively.

To satisfy the orthogonality condition, the coefficients α

and β are determined as follows:

$$\xi_k = \frac{\alpha}{2\omega_k} + \frac{\beta\omega_k}{2} (k = 1,2,\cdots,n) \quad (9)$$

Here, ξ_k represents the damping ratio, while ω_k denotes the natural frequency.

Using finite element software, two natural frequencies ω_i and ω_j can be calculated. Selecting $\omega_i=\omega_1=2.5862$ and $\omega_j=\omega_3=3.6654$,the damping ratios are typically taken as $\xi_i=\xi_j=0.05$. Substituting into equation(9),the coefficients are obtained as: $\alpha=0.95225,\beta=0.00255$.

Interface elements are used to simulate the interaction between the anti-slide pile and the rock mass. The normal stiffness Kn and tangential stiffness Kt for the interface between the anti-slide pile and fractured limestone are set to 6.7×10^{10} MN/m² and 60 MN/m², respectively. The interaction between the anti-slide pile and intact limestone, K_n and K_t are set to 9.6×10^{10} MN/m² and 82 MN/m², respectively. A viscoelastic artificial boundary is used to eliminate or reduce the influence of reflected waves at the finite region boundary. The tangential and normal viscous forces of the dampers are given by:

$$\begin{aligned} t_n &= -p_0 C_P v_n \\ \beta &= -p C_s v_t \end{aligned} \quad (10)$$

Here, p_0 represents the material density at the model boundary, C_P is the P-wave velocity, C_S the S-wave velocity, and v_n and v_t are the normal and tangential velocities of the propagating seismic wave, respectively.

4.3. Selection of Seismic Waves

This study selects the first 25s of the acceleration timeline of the 2008 Wenchuan earthquake recorded at the Chengdu CD2 station (see Fig. 2) to study the stability of the anti-slide pile-reinforced slope under different seismic wave amplitudes. The SeismoSignal software is used to filter and baseline correct the selected Wenchuan earthquake wave. The amplitude of the Wenchuan earthquake wave is adjusted to 0.1g, 0.2g, and 0.3g. The effect of these three seismic levels on the anti-slide pile-reinforced slope is analyzed to reveal the relationship between earthquake magnitude and slope stability.

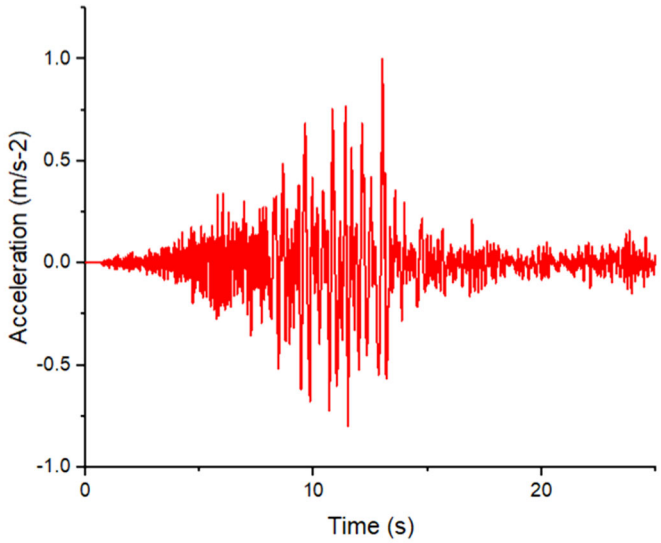

Figure 2. Seismic Acceleration Time History Graph of the Wenchuan Earthquake Wave

5. Results and Analysis

5.1. Seismic Acceleration Study of Slope Reinforced with Anti-Slide Pile

The seismic acceleration time history curves at various monitoring points on the slope surface, under different amplitudes of the Wenchuan earthquake waves, are presented below.

As seen in Fig. 3, the seismic acceleration time history curves at different monitoring locations on the slope surface exhibit certain regularity under different amplitudes of the Wenchuan earthquake waves. Initially, the seismic acceleration at each point on the slope surface is relatively gentle due to the incomplete release of seismic energy. As the seismic energy gradually increases, the seismic acceleration begins to rise rapidly, especially when the seismic amplitude reaches its peak. The amplification effect is more pronounced at higher elevations, where the soil mass is more susceptible to significant vibration, resulting in increased acceleration.

Further analysis shows that the seismic acceleration at different elevations on the slope surface is not uniformly distributed but amplifies with increasing elevation. This amplification effect is more evident at higher elevations due to the greater vibration response of the soil under seismic waves. For example, at monitoring point C, the peak seismic acceleration under a 0.1g seismic wave is 0.674g, increasing to 1.422g under a 0.3g seismic wave. This significant increase in acceleration indicates that the anti-slide pile's effectiveness in stabilizing the upper rock mass of the slope diminishes as the seismic wave amplitude increases, particularly under larger amplitudes, where the control over acceleration growth is limited.

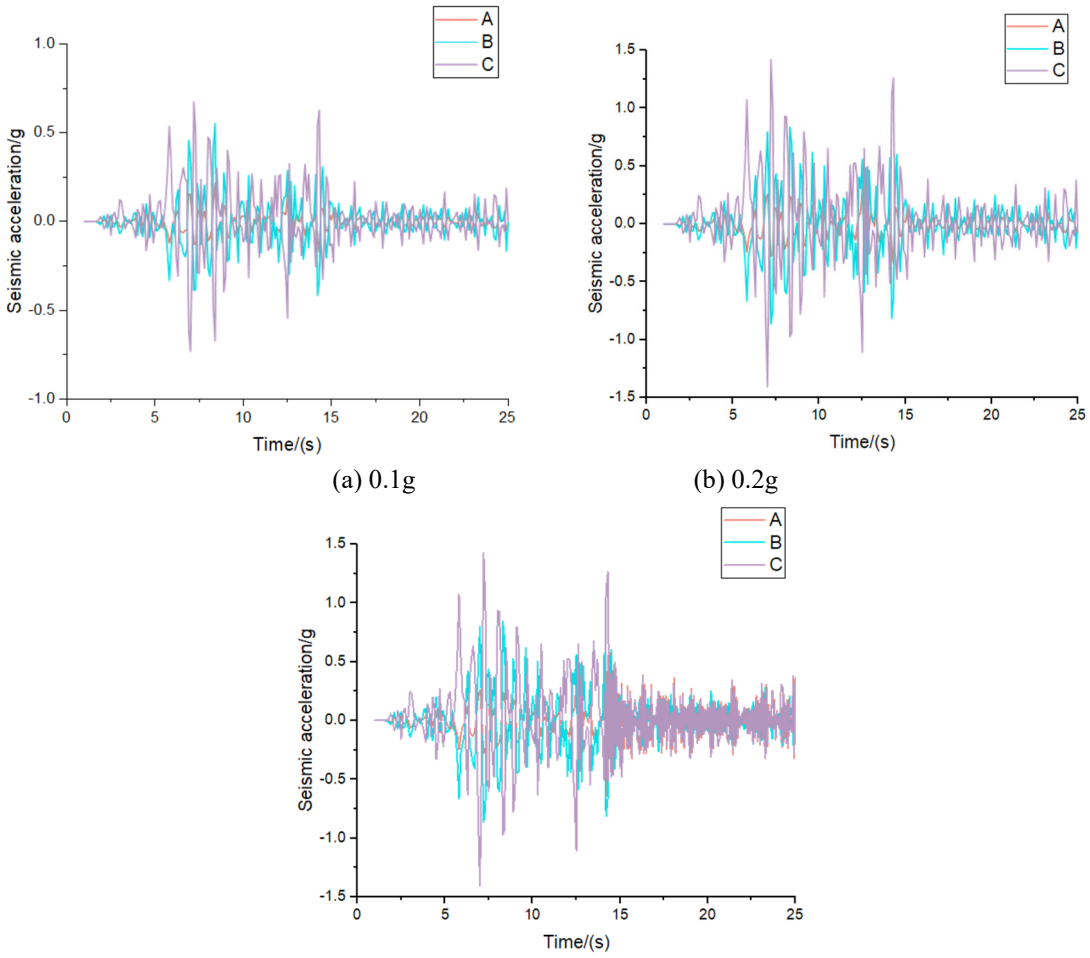

Figure 3. Time History Curves of Seismic Acceleration at Various Monitoring Points under Different Seismic Wave Amplitudes

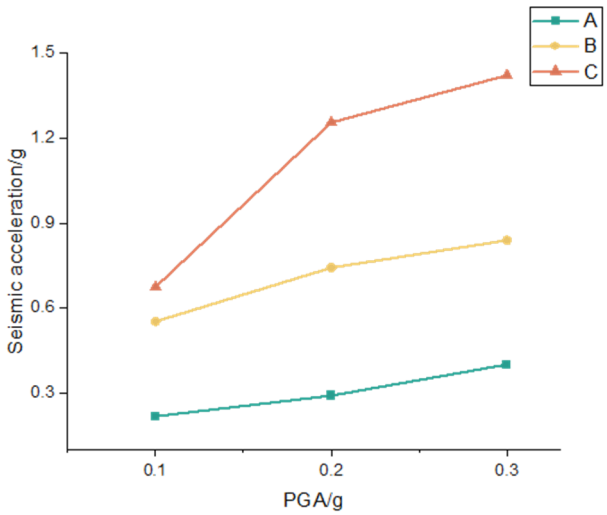

Figure 4. Peak Seismic Acceleration at Various Monitoring Points under Different Seismic Waves

The time history curves of relative horizontal displacement in the x-direction at multiple monitoring points on the slope surface under different amplitudes (0.1g, 0.2g, 0.3g) of the Wenchuan earthquake waves are shown below. The analysis of the relative horizontal displacement in the x-direction under different amplitudes of the Wenchuan earthquake waves reveals a trend in displacement variation over time. Initially, when the seismic wave amplitude is low, the horizontal displacement in the x-direction is minimal, demonstrating that the anti-slide pile effectively restrains the sliding of the slope soil mass during the early stages. However, as the seismic wave amplitude increases, the horizontal displacement in the x-direction begins to increase significantly, particularly when the seismic wave reaches its peak acceleration, resulting in the maximum displacement at every monitoring location on the slope surface.

5.2. Seismic Displacement Analysis of Anti-slide Pile Reinforced Slope

Monitoring points A, B, and C are located on the slope surface, as illustrated in Figure 1. As seen in Figure 5, under

different amplitudes (0.1g, 0.2g, 0.3g) of the Wenchuan earthquake waves, The relative horizontal displacement in the x-direction along the slope surface varies with elevation, increasing as elevation rises rather than being uniformly distributed. Specifically, at higher elevations, the displacement peak is relatively larger, indicating that the soil mass at higher elevations is more prone to sliding under seismic wave action. For example, at monitoring point C, the peak displacement under a 0.3g seismic wave reaches 530.516mm, while the peak displacements at monitoring points B and A are 304.22mm and 184.132mm, respectively. This indicates that the anti-slide pile's effectiveness in restraining the sliding of the upper soil mass of the slope is still insufficient, particularly under larger seismic amplitudes, where the slope's stability may be significantly challenged.

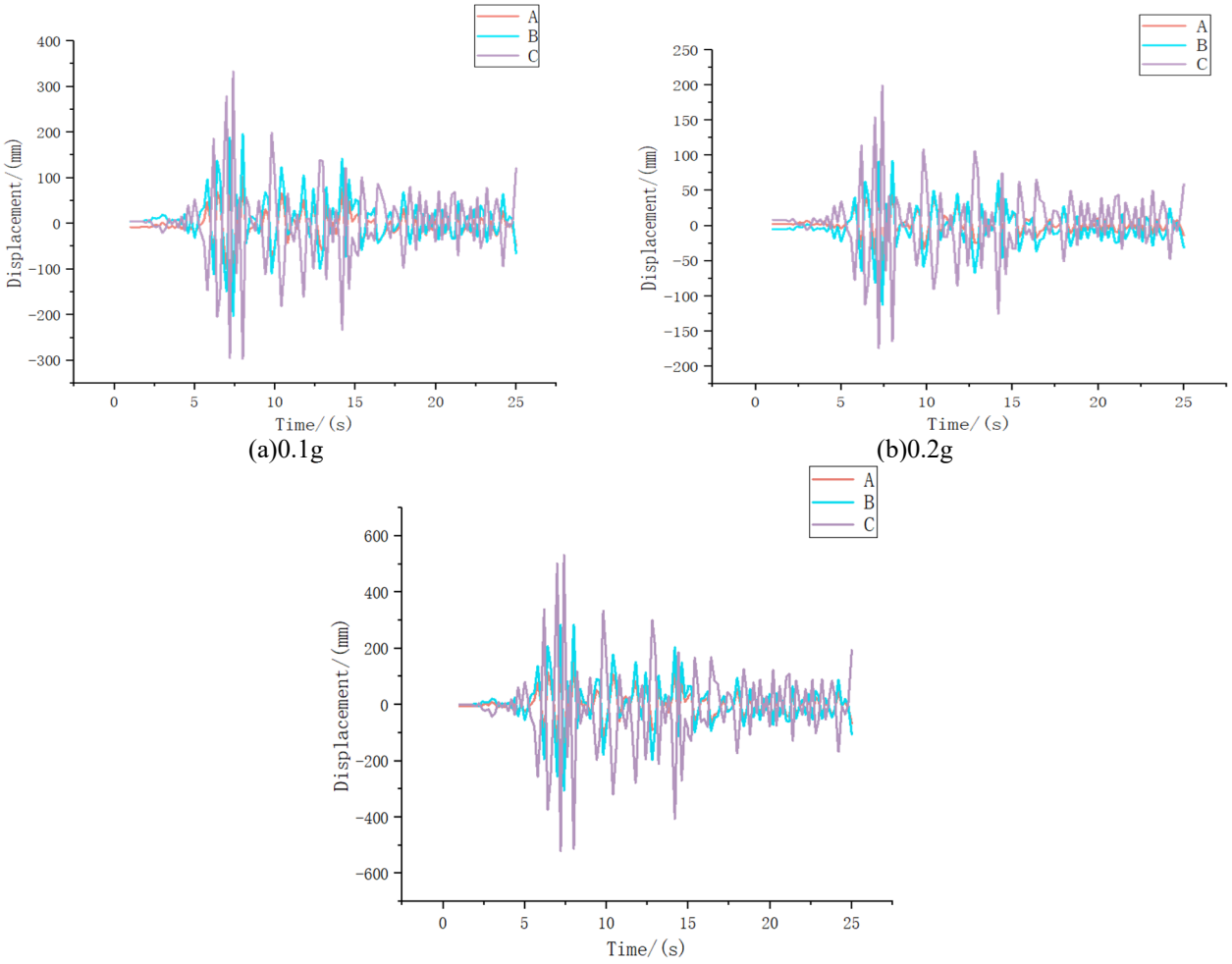

(a)0.1g (b)0.2g

(c)0.3g

Figure 5. Time History Curves of Seismic Displacement at Various Monitoring Points under Different Seismic Wave Amplitudes

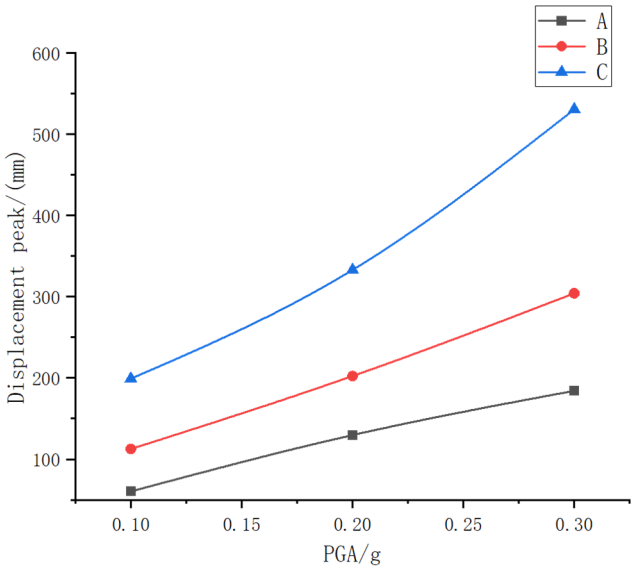

Figure 6. Peak Seismic Displacement at Various Monitoring Points under Different Seismic Waves

Analyzing peak horizontal displacements in the x-direction across multiple monitoring points on the slope surface under different anti-slide pile setups indicates that, at a 0.3g seismic wave amplitude, the peak displacement at monitoring point C (530.516mm) is greater than at point B (304.22mm) and point A (184.132mm). This indicates that the anti-slide pile effectively restrains the sliding of the upper soil mass of the slope, reducing the risk of slope instability under seismic action.

5.3. Analysis of Seismic Principal Stresses in Slope Reinforced by Anti-Slide Pile

The distribution of the first principal stress of the anti-slide pile under different seismic wave amplitudes is shown in Fig. 7.

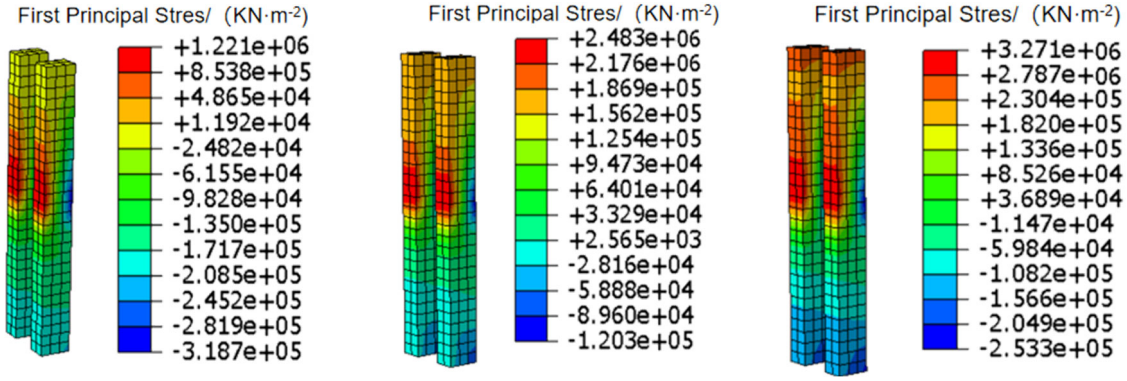

(a) 0.1g (b) 0.2g (c) 0.3g

Figure 7. First Principal Stress Distribution of Skid Pile under Different Seismic Wave Amplitudes

The distribution pattern of the first principal stress on the anti-slide pile under various seismic wave amplitudes shows that the principal stress is focused around the connection between the sliding surface and the anti-slide pile. This stress concentration is mainly due to the slope's sliding tendency under seismic forces. During the earthquake, the anti-slide pile not only bears the active earth pressure from within the slope but also resists the passive earth pressure from outside. These complex force systems are transmitted through the anti-slide pile to the vicinity of the sliding surface, leading to a sharp increase in stress in this region.

As seen in Figure 7, the first principal stress of the anti-slide pile is mainly concentrated near the connection between the sliding surface and the anti-slide pile. At varying seismic wave amplitudes, the first principal stress of the anti-slide pile is 1.221MPa (0.1g), 2.483MPa (0.2g), and 2.271MPa (0.3g). The anti-slide pile interacts with the sliding surface and the surrounding soil mass by embedding into the slope, forming a system that resists sliding. The change in stress indicates that under larger seismic amplitudes, the stress concentration in the middle region of the anti-slide pile is more pronounced, suggesting that the structure may bear significant deformation pressure. Therefore, the structural design of the anti-slide pile should particularly strengthen the middle region to address the stress concentration under seismic action.

6. Conclusion

Based on the background of an actual engineering project, this study established a three-dimensional finite element model of an anti-slide pile-reinforced slope under different seismic wave amplitudes. The slope's stability under seismic forces was examined, with an analysis of the movement patterns, seismic acceleration, and the first principal stress distribution in the anti-slide pile. The following conclusions were drawn:

The dynamic displacement variation trends at different elevation points are essentially the same. The horizontal displacement in the x-direction at multiple monitoring points on the slope surface increases with the seismic acceleration amplitude, with the peak appearing around 7.56s, slightly later than the peak seismic acceleration time. The anti-slide pile effectively restrains the sliding of the upper soil mass of the slope, reducing the risk of slope instability under seismic action.

The seismic acceleration at different locations on the slope surface increases with elevation, exhibiting a certain amplification effect. The effect of amplification becomes more significant with higher slope elevation.

The first principal stress of the anti-slide pile primarily concentrated near the connection between the sliding surface and the anti-slide pile, requiring reinforcement of the structural design in the middle region of the anti-slide pile.

Under 0.1g and 0.2g seismic conditions, the stability coefficient of the anti-slide pile meets the standard requirements. However, under 0.3g seismic conditions, the stability coefficient of 1.095 is less than the standard requirement of 1.10, indicating that the use of anti-slide piles alone as a slope reinforcement form is insufficient and requires improvements to the structure's design or dimensions.

References

[1] Tang Yunbo. Study on Seismic Dynamic Response of Powdery Clay Slope Supported by Prestressed Anchor Cable Anti Sliding Pile [D]. Chongqing Jiaotong University, 2021. DOI: 10.27671/d.cnki. gcjtc. 2021.000729

[2] Yan Bohua. Simulation analysis of anti sliding pile support slope under earthquake action [J]. Northern Transportation, 2023, (10): 30-33+38. DOI: 10.15996/j.cnki.bfjt.2023.10.008

[3] Hao Jianbin. Research progress on slope stability under earthquake action [J]. World Earthquake Engineering, 2014, 30 (01): 145-153

[4] Luo Yu, He Siming, He Jinchuan. Study on the Mechanism of Anti Sliding Pile under Earthquake Action [J]. Journal of Changjiang Academy of Sciences, 2010, 27 (06): 26-29

[5] Li Shulin, Zhao Ruiming, Peng Fuhua, et al. Stability analysis of high and steep slope landslide control based on strength

reduction method [J]. Journal of Building Science and Engineering, 2020,37 (01): 120-126. DOI: 10.19815/j.jace. 2018.07090

[6] Chen Xing, Chen Wenyu, Song Xinghai, et al. Dynamic response and stability analysis of curved skid pile reinforced slopes under earthquake action [J]. Safety and Environmental Engineering, 2020, 27 (04): 79-86+101. DOI: 10.13578/j.cnki. issn. 1671-1556.2020.04.011